

Cite this: *Soft Matter*, 2011, **7**, 11380

www.rsc.org/softmatter

PAPER

Solution scattering studies on a virus capsid protein as a building block for nanoscale assemblies†

Marta Comellas-Aragonès,^a Friso D. Sikkema,^a Guillaume Delaittre,^a Ann E. Terry,^b Stephen M. King,^b Dirk Visser,^{b,c} Richard K. Heenan,^b Roeland J. M. Nolte,^a Jeroen J. L. M. Cornelissen^{ad} and Martin C. Feiters^{*a}

Received 15th June 2011, Accepted 30th September 2011

DOI: 10.1039/c1sm06123b

Self-assembled protein cages are versatile building blocks in the construction of biomolecular nanostructures. Because of the defined assembly behaviour the cowpea chlorotic mottle virus (CCMV) protein is often used for such applications. Here we report a detailed solution scattering study of the CCMV virus and empty capsid. Contrast variation in small-angle neutron scattering (SANS) reveals a well-defined protein shell, with RNA associated mainly with its inner surface. The empty capsid has a protein shell with a diameter comparable to that of the virus, and has some weak scattering density associated on the inside, presumably the N-terminal part which is involved in RNA binding. Dynamic light scattering (DLS) and SANS show that the virus swells with increasing pH (5.0 to 7.5), whereas the empty capsid disassembles; the aggregation behaviour of the capsid protein becomes more complex at salt concentrations below 0.5 M NaCl. Incorporation of polystyrene sulfonate (PSS) in the capsid gives a particle with a solvent core, a polymer inner shell, and a protein outer shell, with a much smaller capsid outer diameter.

1 Introduction

Virus protein-based assemblies find increasing application in the formation of (functional) nanostructures. In this emerging field, sometimes referred to as *chemical virology*, rod-like viruses are used to organize enzymes¹ and chromophores² and to direct crystal growth.³ On the other hand, spherical viruses have been used as containers to direct or confine mineralization^{4–6} and as a nanoreactor when enzymes are encapsulated.^{7–10} In particular for the latter application, detailed insight in the solution properties of the protein cages is helpful. In our recent studies towards a virus-based nanoreactor, we have employed the capsid (*i.e.*, the protein cage without genetic

material, assembled from the coat protein, CP) of the Cowpea Chlorotic Mottle Virus (CCMV). It turns out that the constituent protein can arrange into different morphologies depending on the guest molecules added.^{11–15} This prompted us to study the solution behaviour of the CCMV and its capsid (with and without a synthetic polyelectrolyte present) at different pH values and salt concentrations, predominantly by scattering techniques.

The three-dimensional structures of many spherical RNA viruses, such as the CCMV, have been studied by different techniques including negative-staining electron microscopy (EM)¹⁶ and X-ray crystallography.¹⁷ In general CCMV is a well-studied virus and can be considered a model system for other spherical RNA viruses. CCMV (diameter 28 nm) swells at high pH in the absence of Ca^{II} ions, due to the repulsion between its carboxylate groups, while maintaining its overall structure. Under these conditions it displays pores of 2 nm in diameter in its protein shell. The removal of RNA from CCMV and the reassembly of the empty capsid from the constituting coat proteins have been extensively studied under a variety of conditions such as pH and ionic strength, as schematically represented in Fig. 1.^{18–28} The capsid is an assembly of 180 identical protein units that assemble into stable dimers, which in turn organize themselves into a T = 3 structure of icosahedral symmetry, that is, a cluster with faces consisting of protein hexamers and pentamers. Techniques such as X-ray crystallography, electron microscopy, gel filtration (*e.g.*, fast protein liquid chromatography (FPLC)), and more recently mass spectrometry,^{29,30} atomic force microscopy (AFM),^{31,32} and dynamic light scattering

^aDepartment of Organic Chemistry, Institute for Molecules and Materials, Faculty of Science, Radboud University Nijmegen, Heyendaalseweg 135, 6525, AJ, Nijmegen, The Netherlands. E-mail: m.feiters@science.ru.nl; Fax: +31.24.3652929; Tel: +31.24.3652016/2676

^bLarge Scale Structures Group, ISIS Pulsed Neutron & Muon Source, Science & Technology Facilities Council, Rutherford Appleton Laboratory, Harwell Science and Innovation Campus, Didcot, OX11 0QX, United Kingdom

^cNWO Physics, present address: Reactor Institute Delft, Department RRR, Section FAME, Delft University of Technology, Mekelweg 15, 2629JB Delft, The Netherlands

^dPresent address: Laboratory for Biomolecular Nanotechnology, University of Twente, Enschede, The Netherlands

† Electronic Supplementary Information (ESI) available: Discussion of effect of D₂O on virus and capsid, FPLC chromatograms, log(I) vs. log(q) version of Fig. 5, r-profile of SANS simulations with scattering length density gradients, Tables with Additional SANS simulation parameters and Buffer compositions. See DOI: 10.1039/c1sm06123b/

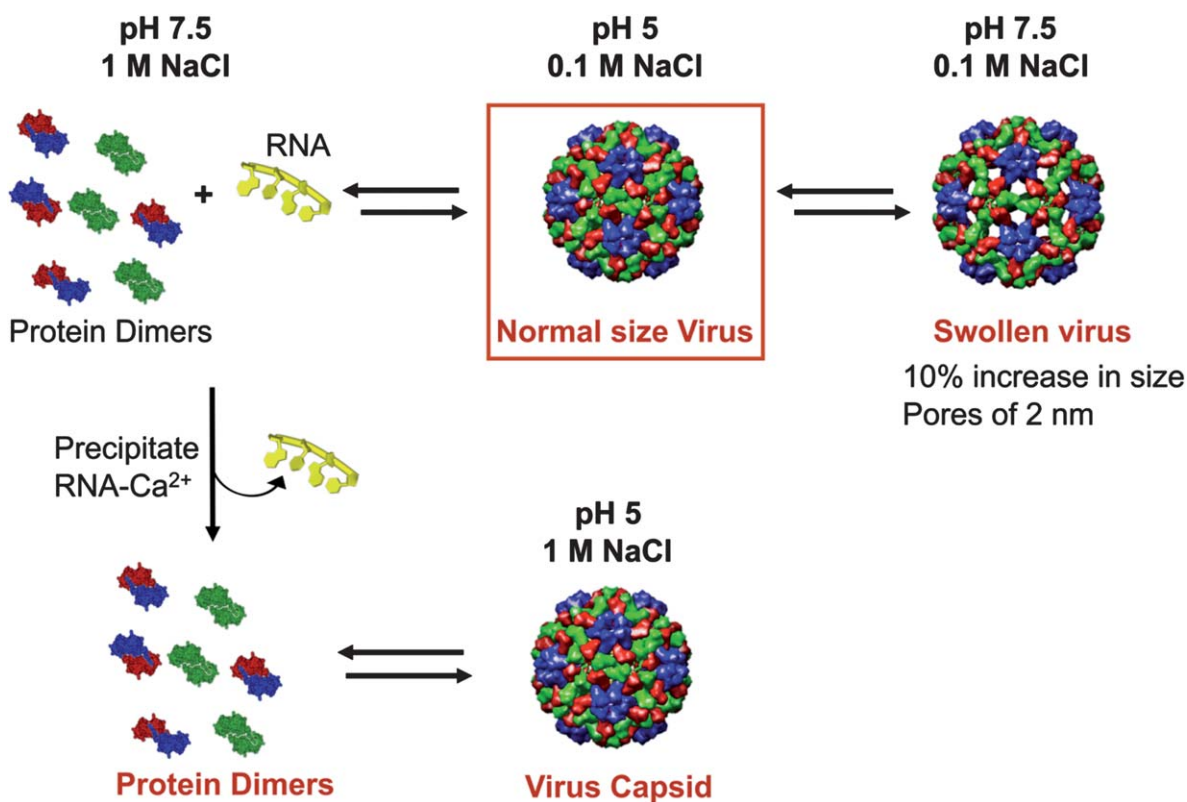


Fig. 1 Assembly pathway of CCMV and the CCMV capsid depending on the pH and ionic strength. Virus images from VIPERdb.²⁸

(DLS)^{33–35} have proven to be valuable tools for the study of viruses and biohybrid assemblies of viruses. Although these techniques have yielded valuable and specific information, we felt that additional knowledge about the size and shape of CCMV and the CCMV capsid and the effect of parameters like pH, salt concentration, removal of RNA, and addition of polymers might be obtained from small-angle neutron scattering (SANS) studies,^{36,37} in particular with regard to the shape and distribution of (i) the protein and RNA in the complete virus, (ii) the protein in the empty capsid, and (iii) the protein and polymer in the biohybrid assembly. The general advantage of solution scattering studies over other techniques like X-ray crystallography and non-cryo electron microscopy is that the solution environment is much closer to the biomolecules' natural environment than the crystal or the sample obtained by drying and staining. The first SANS study on the protein–nucleic acid organization of a number of RNA viruses³⁸ confirmed the structure of the viruses obtained by other techniques, but furthermore provided a consistent set of data, from which low-resolution models could be built. It was concluded that there are differences between these viruses with respect to the degree of interpenetration of the RNA into the protein shells, related to the nature of the forces stabilizing the virus. Following this pioneering study, many other viral particles have been investigated by SANS, of which the bromegrass mosaic virus (BMV)^{39–41} is most closely related to CCMV. Using the contrast variation method as discussed in detail in section 2.4, SANS can nicely complement X-ray crystallographic studies to provide low-resolution information on the radial distribution of protein and

RNA in a virus, and the possible reorganization that occurs upon swelling or disassembly of the virus. The method is generally applicable and allows a simple systematic comparison between viruses.³⁸

The present work starts with a study of the dependence of the structures of CCMV and the CCMV CP on pH and ionic strength by conventional techniques such as FPLC and TEM. The results are schematically represented in Fig. 1. We then describe SANS studies on CCMV, which were carried out to see whether this technique would confirm the structural data obtained by other techniques and provide us with additional information about the CCMV structure. Subsequently, we have used SANS, including the contrast variation method, to analyze a biohybrid assembly composed of the CCMV capsid and polystyrene sulfonate (PSS).¹³ Furthermore, in parallel to the SANS measurements, DLS studies have been performed to complement the SANS data and to test the postulated models. The combination of these two non-destructive techniques gives additional information about CCMV, its assembly properties, and the structure of the biohybrid particles. This work is of interest as a multidisciplinary study of a particle that has been well characterized by a number of other techniques. Detailed information on the structures of the virus and the capsid with and without polymer is important, not only because of their biological significance, but also in view of the aforementioned promising applications of viral capsids as templates for the preparation of (polymer) nanoparticles of well-defined size and shapes, and as containers in which enzymes and other catalysts can be combined to form nanoreactors.

2 Experimental and theoretical background

2.1 Chemicals

Sodium acetate trihydrate (>99%) and uranyl acetate dihydrate ($\geq 98\%$) were purchased from Fluka. Ethylenediaminetetraacetic acid disodium salt dihydrate (EDTA) (>99%), tris(hydroxymethyl)aminomethane (Tris) (>99%), calcium chloride dihydrate (>99%), sodium chloride (99.5%), and sodium azide (99%) were purchased from Acros. Phenylmethanesulfonyl fluoride (PMSF) ($\geq 98.5\%$) and dithiothreitol (DTT) (99%) were obtained from Sigma-Aldrich.

2.2 Virus isolation and capsid preparation

Isolation of CCMV and CCMV coat protein (CP). The purification of the CCMV and the CCMV CP isolation were performed as described earlier.^{7,13,26} The approximate concentrations of the virus and the capsid in the initial stock solutions were 10–15 mg mL⁻¹ and 4–8 mg mL⁻¹, respectively. Two different sets of SANS experiments were performed by using two different virus and CP batches. The concentrations were intended to be as similar as possible within the range described above.

Preparation of CCMV and CCMV capsid samples under different pH and ionic strength conditions. To prepare the SANS samples, different aliquots of CCMV and CCMV CP stock solutions ($V \approx 500 \mu\text{L}$) were dialyzed (M_W cut-off 12 000–14 000) against the corresponding buffer in H₂O (see Table S2, ESI[†], for buffer conditions, and the TEM section in 2.3 for details the dialysis). Part of these solutions were kept for analysis of the samples in H₂O and the rest was dialyzed against the same buffer prepared in D₂O. In all cases, the samples were dialyzed against a minimum of two changes of buffer ($V \approx 400 \text{ mL}$; 3 h per change). The background solutions were taken from the last dialysis buffer after the last change, to have exactly the same H₂O/D₂O ratio in the sample and in the background solution. For those buffers containing D₂O, the pH was corrected and corresponded to $\text{pD} = \text{pH} + 0.3314n + 0.0766n^2$, in which n is the volume fraction of D₂O and pH is the pH meter reading.⁴² Buffers and samples were stored at 4 °C and the dialyses were performed in a cold room at 4 °C.

Preparation of PSS-containing particles. CCMV capsid samples with encapsulated PSS were prepared and characterized as described previously.¹³ For the SANS experiments, capsid protein and PSS were dissolved in 100% D₂O buffered at pD 7.5 containing 0.5 M NaCl and mixed to a final concentration of 3.6×10^{-4} and 2.7×10^{-4} M for protein and polymer, respectively.

2.3 Instrumentation

UV/Vis spectroscopy was performed on a Varian Cary 50 spectrophotometer at room temperature using a quartz cuvette (Hellma, light path: 1 cm). The reference spectra of the corresponding buffers were subtracted from all UV/Vis spectra.

Fast protein liquid chromatography (FPLC) was performed on an Ettan Akta LC system equipped with a Superose 6 PC 3.2/30 column from Amersham Biosciences (flow rate 40 $\mu\text{L min}^{-1}$). Injections of 20 mL aliquots of the samples on the FPLC column

at room temperature were monitored by UV/Vis detection at 280 and 260 nm.

Transmission electron microscopy (TEM) micrographs were recorded on a JEOL JEM-1010 instrument. Samples were prepared by drying a drop of the solution on a Formvar carbon-coated grid, which had been previously made hydrophilic by glow discharge. The excess buffer on the grid was blotted away after 1 min with filter paper. Negative staining of the samples was achieved by applying a drop of uranyl acetate solution (0.2% in MilliQ) onto the grid and blotting the excess liquid away after 15 s with filter paper. The samples were left to dry in air for 30 min before analysis. Dialysis was performed by using dialysis tubing (Spectra/Por 4, M_W cut-off 12 000–14 000, Flat width: 25 mm) purchased from Spectrum Laboratories, and D-tube dialyzer (M_W cut-off 12 000–14 000 or 6000–8000, volume: 1000–3000 μL) from Novagen.

Dynamic light scattering (DLS) measurements were carried out on native CCMV or CP solutions at different pH and/or salt concentrations. The concentration ranged from 0.16 to 1.6 mg mL⁻¹ for the CCMV samples and from 0.13 to 1.3 mg mL⁻¹ for the CP samples. The acquisition was performed at 15 °C at an angle of 173° (backscattering mode) with a Zetasizer Nano S from Malvern using a 4 mW He–Ne laser at 633 nm. Analysis of the data was performed using the Nano DTS v.5.10 software. Reported values and graphs have been selected from the experiments in an equilibrium state, that is, when no further change was observed after one day.

SANS measurements were performed on the LOQ beam line⁴³ at the ISIS pulsed neutron source (CCLRC Rutherford-Appleton Laboratory, Didcot, UK). LOQ uses pulses of neutrons of wavelengths between 0.22 and 1.0 nm which are separated by time-of-flight and detected by a 64 × 64 cm, two-dimensional detector at 4.1 m from the sample. Samples were typically exposed for 2.5 to 3 h. Wavelength-dependent corrections were made to allow for the incident spectrum, detector efficiencies, and measured sample transmissions to create a composite SANS pattern (see ref. 43, for a more detailed description). This gives a scattering vector $q = (4\pi/\lambda) \sin(\theta/2)$ in the range of $q = 0.1$ – 2.8 nm^{-1} . Comparisons with scattering from a partially deuterated polystyrene standard allowed absolute scattering cross sections to be determined with an error of $\pm 2.0\%$. Quartz cuvettes with a light path of 2 mm (type 110-QS, Hellma) were used with an 8 mm diameter beam to perform most SANS measurements, except the swelling studies, in which case banjo cells (type 120-QS, Hellma) were used with a 12-mm diameter beam. Cuvettes of 1-mm light path were used for samples containing H₂O.

2.4 SANS and contrast variation

SANS is similar and often complimentary to other scattering techniques, namely, small-angle X-ray scattering (SAXS) and light scattering (LS). In each of these techniques radiation is elastically scattered by a sample and the resulting scattering pattern, which is represented by the intensity as a function of the scattering angle (recalculated as the scattering vector $q = (4\pi/\lambda) \sin(\theta/2)$ (nm^{-1})), is analyzed to provide information about the size and shape of the object. The type of radiation and the way in which this radiation interacts with matter are the main differences between these techniques. Light and X-rays are both scattered by the electrons surrounding the atomic nuclei, but

neutrons are scattered by the nuclei themselves, a fact that has several important consequences.^{36,44} The strength of the neutron–nucleus interaction varies completely irregularly with the atomic number Z ; not even isotopes of the same element have the same neutron-scattering cross-section. The most significant isotopic variation is the one involving hydrogen and deuterium. The different scattering densities of these two isotopes are used in the so-called SANS “contrast variation method”.

This method is very powerful for the investigation of the structure and dynamics of biological systems and related biomaterials.⁴⁵ Isotopic substitution of H for D is routinely used to change the scattering of a biomacromolecule without affecting its biochemistry. Often, this substitution is as simple as using D_2O instead of H_2O in the solvent to increase the contrast between the studied molecules and the solvent and to decrease the background due to the incoherent scattering by H. In complexes composed of two components with different neutron-scattering length densities, the scattering from one component can be separated from the other one by measuring the complex in water containing solvents with different H_2O/D_2O ratios (Fig. 2). This provides unique structural information about each individual component and the way the components interact with each other in the complex.^{36,37} Because of the exchange of acidic protons with the solvent, water, the scattering length density of proteins and polynucleotides varies with the solvent (D_2O/H_2O) composition, whereas that of hydrocarbons like lipids and polystyrene ($\rho = 1.42 \times 10^{-11} \text{ cm nm}^{-3}$) does not.⁴⁴ It can be concluded from Fig. 2 that in 100% D_2O , the contrast between solvent, protein, and hydrocarbon is optimal, whereas for RNA the contrast is better in 100% H_2O . The scattering length densities in Fig. 2 can be transformed into the core–shell and core-2-shell models used to simulate the SANS of virus and capsid represented in Fig. 3.

2.5 SANS data analysis

It has recently been demonstrated that small-angle scattering (X-ray) data can be simulated with the help of the coordinates of

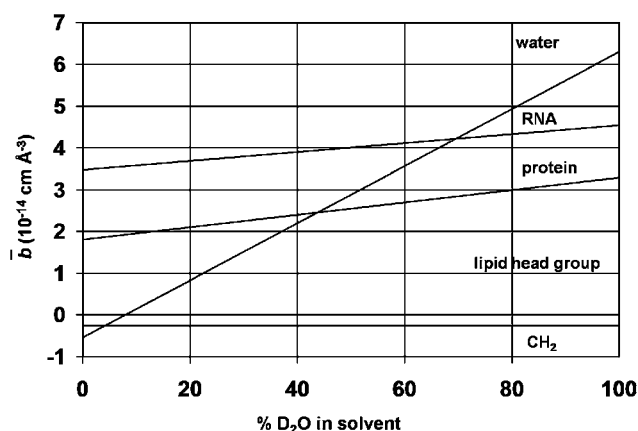


Fig. 2 Average scattering length density for various biological molecules as a function of the D_2O concentration in the solution (adapted from ref. 46). The crossing point of the water line with that of a solute is called the “matching” or isopycnic point.³⁶ The matching points for capsid protein and RNA are 43% and 68% D_2O/H_2O , respectively.

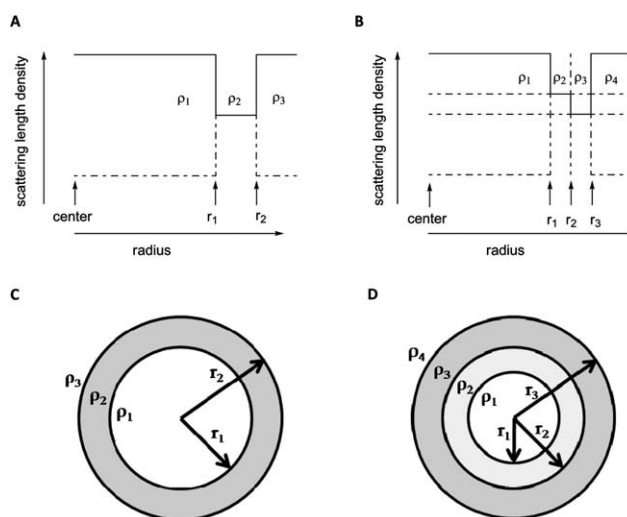


Fig. 3 Schematic scattering length densities in (A, C) core-shell and (B, D) core-2-shell models; the outer shell is polydisperse. In (B), the top horizontal interrupted solid line represents the 100% D_2O level, and the dashed lines from top to bottom indicate the levels of 68, 43, and 0% D_2O , where the solvent scattering length densities match those of RNA, protein, and H_2O , respectively (see also Fig. 2).

the protein structure, for example, as determined by X-ray crystallography.⁴⁷ Such coordinates are available for the CCMV protein,¹⁷ but not for the RNA and the polymer (see below) included in the viral cage. In our calculations of the SANS cross sections we therefore approximated the virus structure with the assumptions (i) that it has spherical symmetry and (ii) that protein, polynucleotide (or polymer), and solvent shells each have a uniform average scattering length density. The SANS model in the programme FISH⁴⁸ included a polydisperse outer radius and shells of fixed thickness, with sharp steps between the shells. The distribution function is a Schultz distribution.⁴⁹ Parts of the fitted value for polydispersity will effectively account for more diffuse boundaries, the approximation of icosahedral shapes by spheres, as well as genuine size or shape polydispersity in re-assembled capsid or capsid plus polymer. The SANS scattering curves were fitted with simple models based on a core-shell or a core with 2 shells, as schematically represented in the top left corners of the corresponding Tables and in Fig. 3, using least squares and Marquardt fits in the programme FISH.⁴⁸ The parameters were refined to give the best agreement with the experimental traces, to extract the optimum values for parameters such as the radius of the particles and the size of the steps in the contrast in the scattering length densities. In this way the optimum values for parameters such as the radius of the particles and the size of the steps in the contrast in the scattering length densities can be determined. In this approximation, the shapes of the virus and capsid are represented as spheres, although the virus is known to have a more complex symmetry, namely, that of an icosahedron. The first model to be applied was a core-shell model, which is characterized by a core with a certain scattering length density ρ_1 (most probably solvent with encapsulated molecules) and a shell with inner and outer diameter r_1 and r_2 and scattering length density ρ_2 (capsid protein, with an RNA and/or polymer component), surrounded by a solvent region with

scattering length density ρ_3 (Table 1, top left, and Fig. 3a and c). In this model, the ρ_2/ρ_3 contrast step was always assumed to be that between protein and solvent ($\Delta\rho = 3.25$ for protein/D₂O), but the step ρ_1/ρ_2 was allowed to float in the refinement, to see if the scattering length density of the core could be identified as solvent, RNA, polymer, or a mixture of these. A selected set of samples were refined with a more complex model (Table 2, top left, and Fig. 3b and d) in which the core was surrounded by an inner and an outer shell of different uniform scattering length density. In these cases, the outer shell was always assumed to be protein, and the contrast step ρ_3/ρ_4 was chosen accordingly, whereas the inner shell could be RNA, polymer, or dilute (“wet”) protein. The scattering curves are presented as the logarithm of the scattered intensity ($\log(I)$) versus the scattering vector (q). This highlights the characteristic features at low q , but also amplifies the experimental noise at high q . The high q part of the scattering curve is used to estimate the level of flat ‘incoherent’ (and multiple inelastic) background scattering that should be incorporated in the simulation; the parts of the curves at $q > 1.9 \text{ nm}^{-1}$ were used in the model fit but omitted from the traces presented in Fig. 5. In our simulations, we have assumed that any effects of interparticle interactions were considered to be negligible at the solution conditions (buffer, ionic strength) used. In the SANS parts of the Results and Discussion section we will first discuss the effect of contrast variation in SANS studies on CCMV, followed by an interpretation with the core-shell model of the scattering data of the virus at different pH values. Subsequently, the SANS results of the CCMV capsid at various salt concentrations and pH values using this same model, along with complimentary DLS studies, will be discussed and compared with the data obtained for the virus. Finally, we will discuss core-2-shell models to interpret the neutron-scattering data of the virus, the empty capsid, and the capsid loaded with PSS.

3 Results and discussion

3.1 CCMV and CCMV capsid assembly as studied by conventional techniques

CCMV at pH 5 is a well-defined monodisperse particle of $d = 28 \text{ nm}$ as shown by TEM (Fig. 4B). The swelling of the virus is clearly demonstrated by FPLC. The virus at pH 5 elutes at $V = 1.1 \text{ mL}$, while at pH 7.5 a peak appears at a smaller elution volume, corresponding to a larger particle (Fig. 4A).

As described in the Introduction (Fig. 1), the viral RNA can be removed from CCMV and the coat protein (CP) isolated. The latter can then be reassembled at pH 5 in the presence of NaCl to form the CCMV capsid, which has dimensions identical to those of the virus. The structure of the reassembled capsid is highly dependent on the pH and salt concentration, as can be concluded from the FPLC and TEM results depicted in Fig. 4. At pH 7.5 the capsid is to a large extent disassembled into protein dimers at salt concentrations between 0.2 and 1.0 M, whereas at pH 5 the salt concentration influences the assembly dramatically, in line with results from the literature (Fig. 4D and G).^{48,21} At low salt concentration ($<0.3 \text{ M NaCl}$), a rather polydisperse distribution of particles is obtained, containing different kinds of larger CP assemblies, that is, lamellar structures or larger capsids, which

elute at $V = 0.8 \text{ mL}$ in the FPLC (Fig. 4D and E). At high salt concentration (higher than 0.3 M), mainly well-defined capsids of $d = 28 \text{ nm}$ are formed, which by TEM show a larger cavity than the virus itself, presumably due to the absence of RNA (Fig. 4G and H). SANS and DLS are techniques that allow the direct study of these assemblies in solution at different pH values and salt concentrations while avoiding sample preparation steps other than dilution.

3.2 SANS contrast variation for CCMV and capsid

The results for the contrast variation studies on CCMV are shown in Fig. 5, left panel, $V100$, $V68$, $V43$, $V0$; the parameters derived from the fits are given in the corresponding entries in Table 1. It can be seen that CCMV gives a scattering curve typical for a (near-)spherical particle such as a virus.³⁸ Solutions of virus in 68 and 43% D₂O (Fig. 5 left, $V68$, $V43$) were prepared to eliminate either the RNA or the protein contribution, respectively.³⁸ At 68% a curve similar to that for 100% D₂O is obtained, as expected for the protein capsid; even the curve at 0% D₂O, where the contrast for RNA is expected to be larger than that for protein, resembles that in 100% D₂O. This apparent resemblance is corroborated by the similarities in the outer radii obtained from the refined fits, which are between 13.0 and 13.5 nm. The values found at the 68% D₂O level, where the RNA contribution is matched, are 10.41 and 13.01 nm for the inner and outer radii, respectively; this is in good agreement with the values found in the crystallographic study (average interior radius 10.4 nm, outer radius between 12.0 nm and to 14.2 nm).² At 43% D₂O, where the contrast is expected to be optimal for RNA, the scattering curve is not well defined. This implies that the RNA structure is disordered to an extent that it can neither be approximated by a shell of the scattering length density of RNA, nor by any other simple structure. When a simulation was attempted, the outer radius refined approximately the same value as that found for the protein shell, which suggests that a residual contrast for the protein contribution is being fitted rather than a genuine RNA contribution. This result was unexpected, because in other viruses studied by SANS, some of which are closely related to CCMV, an RNA shell was clearly present.³⁸ In a combined X-ray crystallography/EM study on CCMV^{11,17} it was found that the regions where the electron density of the RNA is well defined are close to the inner surface of the virus. Under the circumstances where the contrast is not optimized for the protein (100, 43, 0% D₂O), the inner radius is significantly smaller than that found for 68% D₂O and the outer radius slightly larger. A possible interpretation of these observations is that in these cases the innermost part, and even some of the outermost part, of the apparent protein shell has a high RNA content. This could imply that while most RNA is inside the capsid some of it protrudes from the protein shell; it could, however, also be explained by assuming that some regions of the protein have scattering length densities that are significantly different from the average value (Fig. 2, 3) used in our model. Interestingly, in the case of 100 and 0% D₂O, the contrast step $\rho_1 - \rho_2$ for the inner radius of the shell does not refine to the value for the contrast step $\rho_2 - \rho_3$ for the outer shell, which is fixed. This suggests that the core does not consist of pure buffer, but contains a significant amount of material with a higher scattering

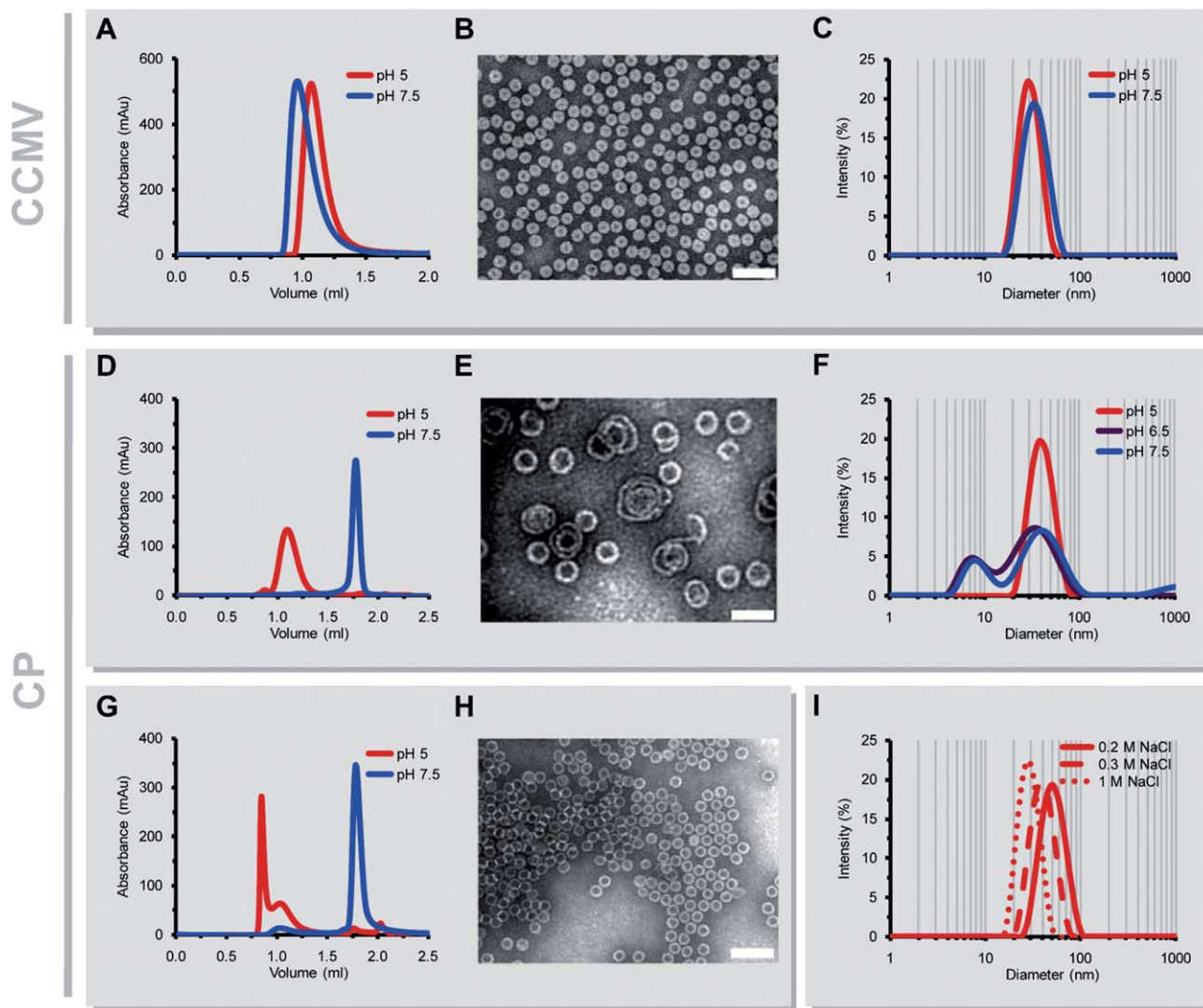


Fig. 4 (A) FPLC of CCMV at pH 5 (compact form) and 7.5 (swollen form). (B) Negative-staining TEM image (bar = 100 nm) of the CCMV virus at pH 5. (C) Size distribution diagrams obtained by DLS for CCMV at pH 5 and 7.5. (D) FPLC traces of the CCMV CP assemblies at 0.2 M NaCl and different pH. (E) Negative-staining TEM image (scale bar = 50 nm) of the CCMV CP at pH 5 at 0.2 M NaCl. (F) Size distribution diagrams obtained by DLS for CCMV CP assemblies at 0.3 M NaCl and different pH. (G) FPLC traces of the CCMV CP assemblies at 1 M NaCl showing the traces at pH 5 and 7.5. (H) Negative-staining TEM image (scale bar = 100 nm) of the CCMV CP at pH 5 at 1 M NaCl. (I) Size distribution diagrams obtained by DLS for CCMV CP at pH 5 and different concentrations of NaCl. Measurements at pH 5 and 7.5 have been depicted with red and blue traces respectively, throughout the Figure.

length density, most likely RNA. For 68% D₂O, where the contrast of the solvent is matched to that of RNA, $\rho_1 - \rho_2$ refines almost to the value fixed for $\rho_2 - \rho_3$, indicating a near-perfect match of the scattering length density of the core with that of the solvent; this is another indication that the core contains some “wet” RNA. The issue of the localization of the RNA in the virus is further discussed in the core-2-shell fits section (see below). Because the CCMV was found to give a better contrast in D₂O than in H₂O, as a result of the fact that the protein contribution is better defined than that of the RNA, it was decided to perform all further studies of the virus and capsid in D₂O. The use of D₂O was found to have no effect on the CCMV and CCMV CP assembly as investigated with FPLC (see Fig. S1, ESI†).

3.3 Swelling of CCMV

In a separate set of SANS experiments with a new sample, the pH-dependent swelling of the virus was studied in detail. The results are shown in Fig. 5 left, *V7.5* and *V5*, and the parameters of the corresponding fits in Table 1. Although care was taken to ensure that the same experimental condition (100% D₂O) was applied to both sets of experiments, differences in r_2 and the polydispersity (PD)) were observed (compare Table 1, entries *V100* and *V5*). The deviations (<2%) are noticeable but are most likely the result of subtle differences in the experimental conditions; the discussion below is focused on data that were obtained on the same batch of biological sample in a single data collection session, such as experiment *V7.5* and *V5*.

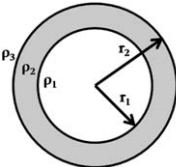
Under the conditions mentioned in Table 1, the swelling of CCMV was detectable by SANS, as is the case for other viruses^{39,50,51} as a shift in the position of the subsidiary maxima to lower q , indicating an increase in the virus radius. This increase (13.14 to 13.71 nm for the outer radius, 9.57 to 10.12 nm for the inner radius) is smaller (4.3% for outer, 5.8% for inner radius) than the 10% swelling observed in earlier X-ray crystallography/EM studies.¹⁷ Complimentary DLS results shown in Fig. 4C also indicated a larger swelling in the hydrodynamic radius (15.29 to

17.30 nm) than that derived for the protein shell radii from the SANS data.

3.4 SANS and DLS studies on the CCMV coat protein at 0.3 M NaCl

SANS experiments on the CCMV capsid, which is expected to dissociate into CP dimers at higher pH, were initially performed at a salt concentration of 0.3 M NaCl. The results are depicted in

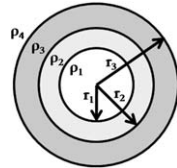
Table 1 Core-shell model fit parameters (r , radius (nm); ρ , contrast (scattering length density, 10^{-11} cm nm⁻³); PD, ((standard deviation)/mean of r_2 , %) of SANS data obtained from experiments with CCMV in solutions of varying D₂O/H₂O composition^a (*V100*, *V68*, *V43*, *V0*) and different pD values^b (*V7.5*, *V5*), and with CCMV CP at different pD values^b at fixed ionic strengths (0.3 M NaCl: *C5-0.3*, *C6.5-0.3*, *C7.5-0.3*; 1.0 M NaCl: *C5-1*, *C7.5-1*) and at different ionic strengths at pD 5 (entries labeled *C*, including *C5-0.2*). The labels in the left column correspond to Fig. 5 (left and middle panel). Top left corner: schematic representation of the core-shell model (see also Fig. 3)



		Expected contrast/result ^d	$\rho_1 - \rho_2$	r_1 (nm)	Δr (nm)	r_2 (nm)	$\rho_2 - \rho_3$ (fixed)	PD (%)
<i>V100</i>	100/0 ^a	protein > RNA	2.75	9.51	3.95	13.46	-3.25	4.09
<i>V68</i>	68/32 ^a	protein	1.31	10.41	2.60	13.01	-1.33	3.59
<i>V43</i>	43/57 ^{a,c}	RNA	-1.33	9.18	4.08	13.26	+1.33	15.69
<i>V0</i>	0/100 ^a	RNA > protein	-2.69	6.12	7.41	13.53	+3.66	23.52
<i>V7.5</i>	pD 7.5	Swollen virus ^d	2.81	10.12	3.59	13.71	-3.25	7.05
<i>V5</i>	pD 5	Virus, $d = 28$ nm ^d	2.80	9.57	3.57	13.14	-3.25	6.27
<i>C5-0.3</i>	pD 5, 0.3 M	Capsid, $d = 28$ nm ^c	3.07	9.94	3.19	13.14	-3.25	7.54
<i>C6.5-0.3</i>	pD 6.5, 0.3 M	(no data) ^{e,d}	3.17	9.20	2.25	11.45	-3.25	13.38
<i>C7.5-0.3</i>	pD 7.5, 0.3 M	CP dimers ^{d,e,f}	3.63	6.74	1.74	8.48	-3.25	23.52
<i>C5-1</i>	pD 5, 1 M	Capsid $d = 28$ nm ^d	3.23	9.48	3.32	12.80	-3.25	8.83
<i>C7.5-1</i>	pD 7.5, 1 M	CP dimers ^{d,g}	3.74	5.44	0.74	6.18	-3.25	31.11
<i>C5-0.2</i>	pD 5, 0.2 M	Capsid $d = 28$ nm ^d	2.83	11.01	2.67	13.67	-3.25	9.00

^a D₂O/H₂O (v/v), buffer: pH or pD 5, 50 mM sodium acetate. ^b Buffers: pD 5, 50 mM sodium acetate; pD 6.5, 50 mM ammonium acetate; pD 7.5, 50 mM Tris-HCl. ^c Data not fitted; simulation of core-shell with low contrast and high polydispersity. ^d Expected on the basis of complementary studies in H₂O, cf. FPLC/TEM in Fig. 4. ^e Parameters for alternative fits with a disc component given in Table S1, ESI. ^f Core-shell model not applicable. ^g Core-shell model not applicable; protein disc with 2.9 nm radius and 2.8 nm thickness included in the fit, to represent the contribution of dimers, in addition to the core-shell contribution with the parameters in the Table.

Table 2 Core-2-shell model simulation parameters (r , radius (nm); ρ , contrast (scattering length density, 10^{-11} cm nm⁻³); PD, ((standard deviation)/mean, %)) of SANS data obtained from experiments with CCMV at different pD values^a (*V7.5*, *V5*), and with CCMV CP at pD 5^d with various ionic strengths (*C5-1*, *C5-0.3*), contrast (*C5-68*) and presence of PSS (*C7.5P10*, *C7.5P2*). The labels in the left column indicate correspondence with the right panel of Fig. 5 and with the experiments for the core-shell fits in Table 1 and Fig. 5 (left and middle panels)



		r_1 (nm)	$\rho_1 - \rho_2$	Δ_{inner} (nm)	r_2 (nm)	$\rho_2 - \rho_3$	Δ_{outer} (nm)	r_3 (nm)	$\rho_3 - \rho_4$	PD (%)
<i>V7.5</i>	CCMV, pD 7.5	4.50	-0.58	6.21	10.71	-2.67	2.84	13.55	3.25	7.10
<i>V5</i>	CCMV, pD 5	4.05	-0.59	5.98	10.03	-2.66	2.99	13.02	3.25	6.28
<i>C5-1</i>	CP pD 5, 1 M	8.43	-0.71	1.59	10.02	-2.54	2.64	12.66	3.25	9.04
<i>C5-0.3</i>	CP pD 5, 0.3 M	9.53	-1.42	0.94	10.47	-1.66	2.62	13.09	3.25	7.56
<i>C5-68</i>	CP pD 5, 0.3 M ^b	9.21	-0.57	0.91	10.12	-0.74	2.89	13.01	1.33	10.13
<i>C7.5P10</i>	CP + PSS-10, pD 7.5, 0.5 M ^c	4.99	-5.20	2.18	7.17	+1.95	1.15	8.32	3.25	15.72
<i>C7.5P2</i>	CP + PSS-2, pD 7.5, 0.5 M ^d	5.14	-4.74	1.54	6.68	+1.49	1.02	7.70	3.25	17.50

^a Buffers: pD 5, 50 mM sodium acetate, pD 7.5, 50 mM Tris-HCl. ^b 68% D₂O. ^c 0.5 M NaCl, PSS M_w 10 000. ^d 0.5 M NaCl, PSS M_w 2000.

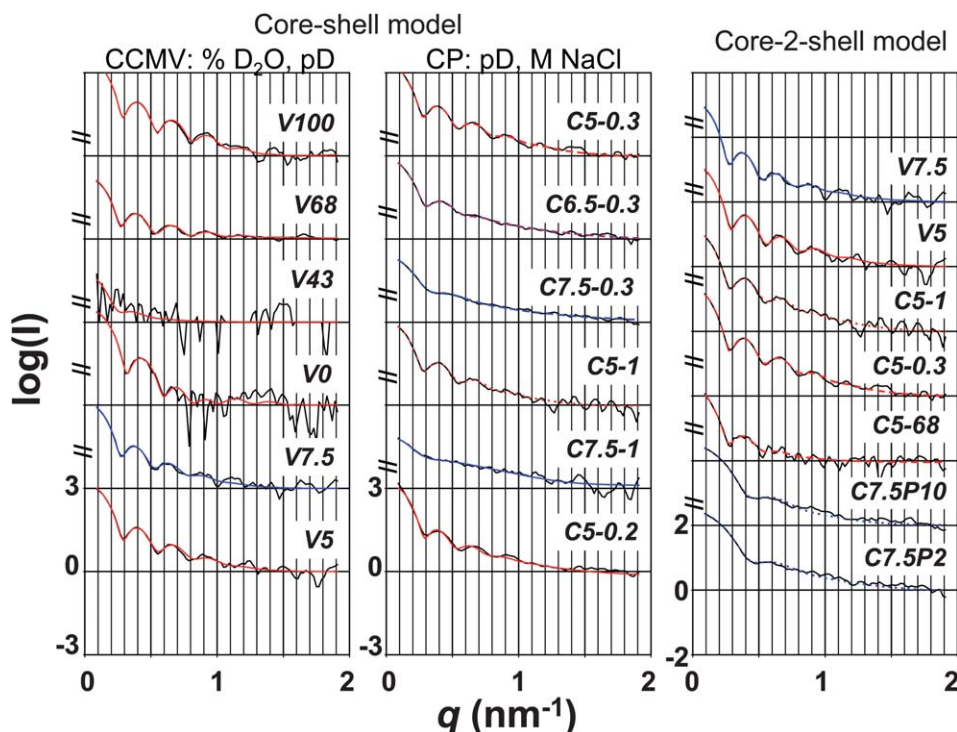


Fig. 5 SANS curves (solid black, experimental; solid colours, fits with the parameters given for the corresponding labels (e.g., *V100*) in Tables 1 (core-shell, left and middle panel) and 2 (core-2-shell, right panel)). Left panel, CCMV with varying contrast (D_2O/H_2O v/v) and pD; middle panel, CCMV CP at various pDs and ionic strengths; right panel, core-2-shell fits of CCMV and capsid with and without polymer. See Tables for the meaning of the labels. Fits at pD 5, pH 6.5, and 7.5 have been depicted with red, violet, and blue traces respectively, throughout the Figure. A $\log(I)$ vs. $\log(q)$ version is given as Fig. S2 in the ESI.†

Fig. 5, *C5-0.3*, *C6.5-0.3*, *C7.5-0.3*, and the parameters of the corresponding fits are presented in Table 1. At pD 5, the capsid has a thinner shell than the virus and slightly larger inner and shorter outer radii, namely, 9.9 and 13.1 nm, respectively. This result is quite close to that obtained for the virus at optimum protein contrast (Fig. 5, *V100*); the structure of the remaining protein shell is the same when the contribution of the RNA to the scattering is minimized in the fits either by removing it or by matching the solvent scattering length density. In the case of the virus, as noted in the contrast study, the contrast step $\rho_1 - \rho_2$ for the inner radius of the shell does not refine to the contrast step $\rho_2 - \rho_3$ for the outer shell, which suggests the presence of some dissolved RNA in the core of the virus (Table 1, entries *V100*, *V7.5*, and *V5*). For the capsid, however, at pD 5 and 6.5, $\rho_1 - \rho_2$ refines to almost the same value as fixed for $\rho_2 - \rho_3$, suggesting that the core contains pure solvent, as expected.

At higher pH, a tendency of the scattering curve maxima to shift to higher q values was observed, indicating a decrease in particle diameter. Concomitant with this shift a damping of the oscillations was found, which indicates either a higher polydispersity or perhaps some variation in shape, i.e., the shell is more elastic.³² The results of the fits reflected this decrease in particle radius and the values (pH 5, 13.1 nm; pH 6.5, 11.5 nm; pH 7.5, 8.5 nm) would point to the occurrence of capsids with $T = 3$ (180 protein units), “ $T = 2$ ” (120 units) and $T = 1$ (60 units) icosahedral symmetry,⁵¹ respectively. Such a result would be unprecedented since all other results (see above) point to a dissociation of the capsid at high pH into CP dimers and not to

the formation of $T = 2$ and $T = 1$ particles. The only report in the literature¹¹ that might be relevant for the present study suggests a swelling of the capsid, not a shrinking. We decided therefore to investigate the samples by DLS to determine if smaller particles were present or not.

The results of the DLS measurements on the CCMV capsid at 0.3 M NaCl are presented in Fig. 4F. At pH 5, the capsid shows a close to perfect homogeneous size distribution, in line with the EM data and the SANS results. The hydrodynamic radius determined from DLS ($r = 19.21$ nm) is somewhat larger than the 13.0–13.5 nm value found with SANS for the outer radius of the protein shell. At pH 6.5, a bimodal distribution is found by DLS, with maxima at diameters of about 8 and 30 nm, indicating the coexistence of CP dimers and whole $T = 3$ capsids. However, because the curve was not corrected for the fact that the DLS intensity is proportional to the volume of the object ($I \propto d^3$), it can be concluded that the solution contains mainly CP dimers, whereas the core-shell simulation for the corresponding SANS would indicate the presence of capsids with a diameter of 23 nm. It has to be noted that the polydispersity in the SANS simulation refines to a relatively high value (13.38%). This might be an indication that the SANS sample also in fact has a bimodal distribution. This is difficult to establish since the contribution of the CP dimers to the SANS curve is not as easy to predict as that of a near-spherical capsid particle. At pH 7.5, the DLS pattern also showed a bimodal distribution and again we assume that the solution contains mainly CP dimers ($d = 7$ –9 nm). This agrees with the results obtained by size-exclusion chromatography

(SEC), whereas the core-shell simulation of the SANS data suggested the presence of particles with a diameter of 17 nm, albeit with an even higher polydispersity (23.52%) than the assembly of particles at pH 6.5. Again it is difficult to decide whether the SANS results at this pH should also be interpreted with a bimodal distribution. An indication that the SANS fits with the core-shell approximation are problematic in this case is the fact that $\rho_1 - \rho_2$ refines to a higher absolute value than the one fixed for $\rho_2 - \rho_3$, which is physically not realistic. It should be noted that for CCMV CP at pH 6.5 and 7.5 fits of equivalent quality to the ones included (entries *C6.5-0.3* and *C7.5-0.3*) in Fig. 5 can be obtained by including a protein disc component to represent the contribution of the capsid protein dimers (see Table S1 in the ESI† for parameters).

From the results presented above it can be concluded that the SANS and DLS studies at 0.3 M NaCl are not conclusive, as DLS gives evidence of a bimodal distribution for cases where the SANS can be simulated with a high polydispersity. pH/Ionic strength phase diagrams based on EM studies in the literature^{21,52} have shown that at an ionic strength of 0.3 M NaCl, the $T = 3$ capsids may be converted to multilamellar capsids at low pH, and the dimers to tubes at high pH. Hence at this ionic strength the coexistence of various species is very likely, and this is not a favorable starting point for the interpretation of the SANS experiments. We decided therefore to continue our studies at an ionic strength of 1 M NaCl, where $T = 3$ capsids and CP dimers are expected to exist at low and high pH, respectively. For the experiments with PSS (see below), a salt concentration of 0.5 M NaCl was chosen in agreement with the conditions reported in literature.^{12,13}

3.5 SANS and DLS studies on the CCMV capsid at high salt concentration

The SANS results for the capsid at high salt concentration, that is, 1 M NaCl, at pH 5.0 and 7.5 are shown in Fig. 5 *C5-1*, *C7.5-1*, with the corresponding parameters derived from the refined fits in Table 1. At pH 5 and 1 M NaCl, the empty capsid is comparable in size to that of the virus, although its outer diameter appears to be slightly (but significantly in terms of the errors in the fit) reduced. The SANS curve of the empty capsid at pH 7.5 (*C7.5-1*) is almost featureless and attempts to simulate it on the basis of a core-shell model gave unreliable results (not shown), with a high polydispersity (>30%) and anomalous contrast steps ($\rho_1 - \rho_2$, 3.74 > $\rho_2 - \rho_3$, 3.25 (fixed)). In the final fit (Fig. 5 *C7.5-1*) a protein disc component was included to represent the contribution of the capsid protein dimer to the SANS. This strongly indicates that the capsid, unlike the virus, does not swell at high pH, but instead dissociates into particles that do not give characteristic contributions to the SANS, presumably CP dimers. This is consistent with our FPLC/TEM results.

In order to better compare the SANS results at high and low salt concentrations and to obtain more information it was decided to carry out additional experiments at a NaCl concentration of 0.2 M. The results for the capsid at pH 5 and at various salt concentrations are compared in Table 1 and Fig. 5, middle (*C5-0.3*, *C5-1*, and *C5-0.2*). When the salt concentration is lowered, a decrease in the shell width of the

capsid (Δr) and an increase in the outer radius (r_2) are observed. This is in agreement with our FPLC/TEM results (Fig. 1, Fig. 4D, E, G, and H), showing that high salt concentrations stabilize the formation of monodisperse $T = 3$ capsids at pH 5, whereas low salt concentrations induce the formation of larger assemblies.

Since the SANS data for the sample containing 0.2 M NaCl could not be fitted very well, we also performed DLS experiments at this ionic strength. In Fig. 4I, the DLS results for the various salt concentrations are compared. The DLS data shows the same trend as the SANS results, except that the capsid diameter shows a clearer increase in size, namely, from 29.0 to 38.4, and further to 49.1 nm, going from 1 to 0.3 and then to 0.2 M NaCl. Unexpectedly, in the DLS analysis all samples seem to have a narrow size distribution, opposite to what was observed by TEM (Fig. 4E). In the latter case, at low salt concentrations a mixture of species with different shapes and dimensions was observed. A possible explanation is that low salt concentrations weaken the interactions between the protein subunits, inducing the formation of larger capsids with thinner shells that are more susceptible to disassembly. During the sample preparation for TEM imaging, this might result in damage and the generation of a variety of species. DLS analysis of CCMV CP at pH 5 containing an even lower concentration of salt (0.1 M NaCl) did show a highly polydisperse mixture of species of different sizes that were not stable over time (not shown). After several minutes a clear scattering curve could no longer be observed and a white precipitate was formed. This points to the formation of large assemblies which, as we checked, were undetectable by FPLC, since their size was beyond the exclusion limit of the FPLC column (Superose 6).

3.6 SANS core-2-shell fits for CCMV and CCMV capsid

The core-shell model used for the interpretation of the SANS experiments so far has led to satisfactory fits for the virus and the capsid under various circumstances, and has given interesting information on the size of the shell, which is dominated by the capsid protein. As for the RNA component of the virus, it has given only indirect information, derived from the differences in the thickness and volume of the shell, and the discrepancy in the inner and outer contrast steps. We considered that it would be interesting to see if the RNA structure could be defined better by simulating the SANS data with a core-2-shell model, consisting of a core, a weakly scattering inner shell (presumably containing dilute RNA and/or protein), and a more strongly scattering outer shell consisting of protein (Table 2, top left corner). In the initial fits of this type, the contrast steps were restrained so that the $\rho_1 - \rho_2$ and $\rho_2 - \rho_3$ steps together were equal in absolute value to the $\rho_3 - \rho_4$ step (which is the protein/D₂O contrast step), though of opposite sign. This situation was retained in the final fits, in which such restraints were removed, indicating that the core-2-shell fits adequately describe a situation where the scattering length density of the core (ρ_1) is equal to that of the surrounding solvent (ρ_4).

In Fig. 5, right panel, the experimental traces and the core-2-shell fits of the SANS data for CCMV and the CCMV capsid are compiled together with the results obtained for capsids with encapsulated PSS (to be discussed in the next section). The

corresponding parameters are given in Table 2, and the corresponding radial scattering length density profiles for CCMV, CCMV capsid, and one of the CCMV capsid-PSS samples in Fig. 6.

For the virus (Fig. 5 right, traces *V7.5* and *V5*; Fig. 6, top trace) the outcome of the core-2-shell simulation approach is a weakly ($\rho_{1,2} = -0.59$) scattering inner shell (4–10 nm) and an outer protein shell (10–13 nm). The latter has an outer diameter that is virtually identical to that found in the core-shell simulation (Table 1), but the inner diameter is approximately 0.5 nm larger. The weakly scattering inner shell can be interpreted as being the result of a dilute solution of RNA bound to the inner surface of the capsid protein. Analysis of the pH-induced swelling of the virus by the core-2-shell model (compare *V7.5* and *V5* in Fig. 5, right, and Table 2) reveals that the aqueous core and the wet RNA shell increase by approximately 0.4 and 0.2 nm in diameter and thickness, respectively. The thickness of the protein shell decreases slightly but its volume still increases somewhat because of the increase in diameter. Presumably, the basic N-terminal part of the capsid protein, the electron density of which is not well defined in the crystal structure,¹⁷ plays a role in the binding of the RNA. Interestingly, simulation of the CCMV capsid with the core-2-shell model (middle trace in Fig. 6, entry *C5* in Fig. 5, right, and Table 2) reveals the presence of a thin (1.0–1.5 nm) weakly scattering inner shell, which could consist of wet protein. The protein nature of this inner shell is corroborated by the finding that the core-2-shell analysis of the empty capsid (0.3 M NaCl) gives the same outcome for measurements performed at 68 (protein contrast selected) and 100% D₂O (entries *C5-0.3* and *C5-68* in Fig. 5, right, and Table 2). The simulation programme FISH allows for adaptations of the core-shell model with an *r*-dependent profile in which the scattering length density varies gradually with *r*. Although the exploration of such more complex models is outside the scope of the present work, we have included the results for fits of

equivalent quality to the ones included (entries *V5* and *C5-0.3*) in Fig. 5 in Fig. S3 of the ESI.† They confirm that well-defined protein shells are present in virus and capsid at pH 5, and that the dilute biomaterial found as an inner shell in the core-2-shell model can be modelled alternatively with a scattering length density which gradually increases from a point in the core towards the outer shell.

3.7 SANS studies on CCMV capsid loaded with PSS by using a core-2-shell model

We have previously shown¹³ that the self-assembling properties of CCMV CP lacking part of its N-terminus can be employed to create a monodisperse 16 nm icosahedral (likely $T = 1$) nanoparticle upon encapsulation of a dispersed negatively charged polymer at pH 7.5. More recent work indicated that these particles can also form from fully intact CP,¹⁴ so more insight in the interaction and organisation of this polyelectrolyte in the capsid is desirable. For the analysis of the SANS data of the capsid with encapsulated PSS,¹³ it turned out that a core-2-shell model approach was vital; these data, therefore, were simulated with a core-2-shell model where the inner shell was a strongly scattering polymer shell ($\rho_1 - \rho_2 = \text{approx. } -5 \times 10^{-11} \text{ cm nm}^{-3}$) and the outer shell a comparatively weakly scattering protein shell ($\rho_3 - \rho_4 = 3.25 \times 10^{-11} \text{ cm nm}^{-3}$). This situation is the reverse of that for the native virus, where the inner (RNA) shell scatters weakly compared to the outer (protein) shell, *cf.* Fig. 6 right. In the initial simulations of this type, the contrast steps were restrained so that the $\rho_2 - \rho_3$ and $\rho_3 - \rho_4$ steps together were equal to the $\rho_1 - \rho_2$ step (which is the PSS-D₂O step). As in the case of the virus, these contrast steps were equal even when such restraints were removed in the final fits (for example for *C7.5P10*, $1.95 + 3.25 = 5.20 \times 10^{-11} \text{ cm nm}^{-3}$); this indicates that the situation where the scattering length density of the core (ρ_1) is equal to that of the surrounding solvent (ρ_4) is adequately described by these core-2-shell fits. In Fig. 5, right, traces *C7.5P10* and *C7.5P2*, the experimental traces and the core-2-shell fits of the SANS data for capsids with encapsulated PSS, are shown. The corresponding parameters are given in Table 2, and the corresponding radial scattering length density profile of one of the CCMV capsid-PSS samples in Fig. 6, bottom trace. The SANS experiments show that the incorporation of the PSS in the CCMV capsid leads to much smaller and more polydisperse particles than those found for virus and capsid (Fig. 6); the outer radii calculated for the two samples (*C7.5P10* and *C7.5P2*) are in the 7.5–8.5 nm range and the polydispersities range from 15 to 18%. This is in line with the earlier conclusion from EM and DLS that the incorporation of PSS presumably leads to the formation of $T = 1$ rather than $T = 3$ capsids.^{12–14} The SANS data allow us to define the polymer and protein shells more precisely. There is an inner solvent core with a radius of around 5.0 nm. This core is surrounded by a polymer shell of 1.5 nm in the case of the PSS of molecular weight M_w 2000 (*C7.5P2*), and 2.2 nm for the PSS of molecular weight M_w 10,000 (*C7.5P10*) and a protein shell of 1.0 nm in both cases. Interestingly, the PSS appears to have a much stronger effect on the capsid structure than RNA; a more condensed structure than the original virus appears, which, however, still has a well-defined but thinner shell of protein with a smaller outer diameter.

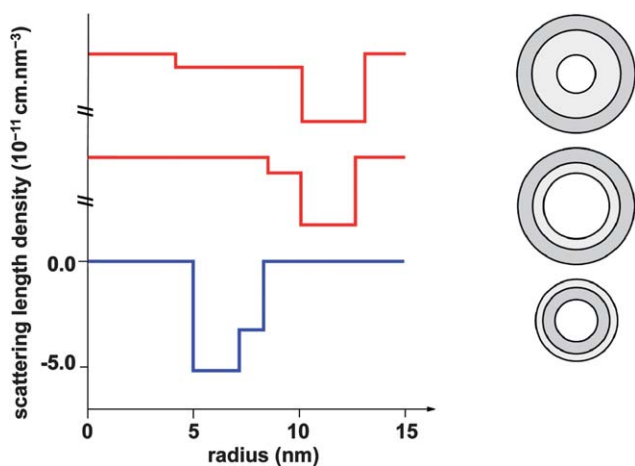


Fig. 6 (left) Scattering length density profiles (relative to 100% D₂O which is arbitrarily set to 0 cm nm⁻³) derived from the core-2-shell fits carried out on SANS data obtained for (top, *V5*) CCMV, (middle, *C5*) CCMV capsid, and (bottom, *C7.5P10*) CCMV capsid loaded with PSS (M_w 10 000); (right) corresponding cross-sections of the mean outer radius spheres with the shells shaded according to relative scattering length density.

4 Conclusions

SANS has allowed us to study the CCMV structure in solution under various pH and salt concentration conditions. The optimum contrast was achieved in D₂O buffers, and the protein component could be defined as a separate shell in the core-shell fits (outer radius 13 nm). Only indirect information could be obtained on the way the RNA molecules are arranged in the virus; most of it is diluted with water and associated with the inside of the protein shell. The swelling of the virus upon changing the pH from pH 5 to 7.5 was detectable, but not as strong as the 10% swelling derived from DLS, EM, and X-ray crystallography. The protein shell of the empty capsid was of a size comparable to that of the virus (marginally smaller) and had some weak scattering density associated on the inside, presumably the N-terminal part which is involved in RNA binding; it was found to dissociate upon increasing the pH. It was necessary to work at concentrations of 0.5 M NaCl and above with the capsid protein to avoid complications due its tendency to form more complex aggregates at low salt concentration. DLS indicated a bimodal size distribution (capsids and capsid protein dimers) at pH values 6.5–7.5 and 0.3 M NaCl. Incorporation of PSS in the CCMV capsid led to the formation of smaller capsids (outer radius 8 nm), predominantly corresponding to T = 1 geometry, with a solvent core, a polymer inner shell, and a protein outer shell.

These results on the solution structure of the CCMV CP highlight the applicability of the material in the formation of functional nanostructures. It is, however, also clear that care should be taken with the exact solvent conditions as different types and mixtures of architectures are formed at intermediate salt concentrations. Furthermore, the encapsulation of the synthetic polyelectrolyte PSS shows that applying a ‘scaffolding’ molecule might lead to some degree of control of the protein assembly.^{14,15}

Acknowledgements

This work was supported by the Netherlands Organization for Scientific Research (NWO) by a TOP grant to R. J. M. N. and a Vidi grant to J. J. L. M. C. through its Chemical Council (NWO-CW), and by supporting experiments at the ISIS Pulsed Neutron & Muon Source of the STFC Rutherford Appleton Laboratory, as well as by the Royal Netherlands Academy for Arts and Sciences (KNAW). Contributions to the Zetasizer by Dutch Technology Foundation (STW) and NanoNed are also acknowledged.

Notes and references

- N. Crette, H. Engelkamp, E. Akpa, S. J. Pierre, N. R. Cameron, P. C. M. Christianen, J. C. Maan, R. Weberskirch, A. E. Rowan, R. J. M. Nolte, T. Michon and J. C. M. van Hest, *Nat. Nanotechnol.*, 2007, **2**, 226.
- P. G. Holder and M. B. Francis, *Angew. Chem., Int. Ed.*, 2007, **46**, 4370.
- Y. J. Lee, H. Yi, W. J. Kim, K. Kang, D. S. Yun, M. S. Strano, G. Ceder and A. M. Belcher, *Science*, 2009, **324**, 1051.
- T. Douglas and M. Young, *Adv. Mater.*, 1999, **11**, 679.
- T. Douglas, E. Strable, D. Willits, A. Aitouchen, M. Libera and M. Young, *Adv. Mater.*, 2002, **14**, 415.
- A. de la Escosura, A. M. Verwegen, F. D. Sikkema, M. Comellas-Aragones, A. Kirilyuk, T. Rasing, R. J. M. Nolte and J. J. L. M. Cornelissen, *Chem. Commun.*, 2008, 1542.
- M. Comellas-Aragones, H. Engelkamp, V. I. Claessen, N. A. J. M. Sommerdijk, A. E. Rowan, P. C. M. Christianen, J. C. Maan, B. J. M. Verduin, J. J. L. M. Cornelissen and R. J. M. Nolte, *Nat. Nanotechnol.*, 2007, **2**, 635.
- J. D. Fiedler, S. D. Brown, J. L. Lau and M. G. Finn, *Angew. Chem., Int. Ed.*, 2010, **49**, 9648.
- I. J. Minten, V. I. Claessen, K. Blank, A. E. Rowan, R. J. M. Nolte and J. J. L. M. Cornelissen, *Chem. Sci.*, 2011, **2**, 358.
- B. Worsdorfer, K. J. Woycechowsky and D. Hilvert, *Science*, 2011, **331**, 589.
- T. Douglas and M. Young, *Nature*, 1998, **393**, 152.
- Y. F. Hu, R. Zandi, A. Anavitarte, C. M. Knobler and W. M. Gelbart, *Biophys. J.*, 2008, **94**, 1428.
- F. D. Sikkema, M. Comellas-Aragones, R. G. Fokkink, B. J. Verduin, J. J. L. M. Cornelissen and R. J. M. Nolte, *Org. Biomol. Chem.*, 2007, **5**, 54.
- R. D. Cadena-Nava, Y. F. Hu, R. F. Garmann, B. Ng, A. N. Zelikin, C. M. Knobler and W. M. Gelbart, *J. Phys. Chem. B*, 2011, **115**, 2386.
- A. de la Escosura, P. G. A. Janssen, A. P. H. J. Schenning, R. J. M. Nolte and J. J. L. M. Cornelissen, *Angew. Chem., Int. Ed.*, 2010, **49**, 5335.
- A. C. Steven, P. R. Smith and R. W. Horne, *J. Ultrastruct. Res.*, 1978, **64**, 63.
- J. A. Speir, S. Munshi, G. J. Wang, T. S. Baker and J. E. Johnson, *Structure*, 1995, **3**, 63.
- J. B. Bancroft and E. Hiebert, *Virology*, 1967, **32**, 354.
- J. B. Bancroft, G. J. Hills and R. Markham, *Virology*, 1967, **31**, 354.
- J. B. Bancroft, G. W. Wagner and C. E. Bracker, *Virology*, 1968, **36**, 146.
- R. F. Bruinsma, W. M. Gelbart, D. Reguera, J. Rudnick and R. Zandi, *Phys. Rev. Lett.*, 2003, **90**, 248101.
- J. T. Finch and J. B. Bancroft, *Nature*, 1968, **220**, 815.
- J. M. G. Fox, G. Wang, J. A. Speir, N. H. Olson, J. E. Johnson, T. S. Baker and M. J. Young, *Virology*, 1998, **244**, 212.
- E. Hiebert, J. B. Bancroft and C. E. Bracker, *Virology*, 1968, **34**, 492.
- E. Hiebert and J. B. Bancroft, *Virology*, 1969, **39**, 296.
- B. J. M. Verduin, *FEBS Lett.*, 1974, **45**, 50.
- M. Young, D. Willits, M. Uchida and T. Douglas, *Annu. Rev. Phytopathol.*, 2008, **46**, 361.
- <http://vipperdb.scripps.edu/>; M. Carillo-Tripp, C. M. Shepherd, I. A. Borelli, S. Venkataraman, G. Lander, P. Natarajan, J. E. Johnson, C. L. Brooks III and V. S. Reddy, *Nucleic Acids Res.*, 2009, **37**, D436.
- C. Uetrecht, C. Versluis, N. R. Watts, W. H. Roos, G. J. Wuite, P. T. Wingfield, A. C. Steven and A. J. Heck, *Proc. Natl. Acad. Sci. U. S. A.*, 2008, **105**, 9216.
- C. Uetrecht, C. Versluis, N. R. Watts, P. T. Wingfield, A. C. Steven and A. J. Heck, *Angew. Chem., Int. Ed.*, 2008, **47**, 6247.
- W. S. Klug, R. F. Bruinsma, J. P. Michel, C. M. Knobler, I. L. Ivanovska, C. F. Schmidt and G. J. Wuite, *Phys. Rev. Lett.*, 2006, **97**, 228101.
- J. P. Michel, I. L. Ivanovska, M. M. Gibbons, W. S. Klug, C. M. Knobler, G. J. Wuite and C. F. Schmidt, *Proc. Natl. Acad. Sci. U. S. A.*, 2006, **103**, 6184.
- H. H. J. Bink and C. W. A. Pleij, *Arch. Virol.*, 2002, **147**, 2261.
- P. Dobos, R. Hallett, D. T. Kells, O. Sorensen and D. Rowe, *J. Virol.*, 1977, **22**, 150.
- Y. Panyukov, I. Yudin, V. Drachev, E. Dobrov and B. Kurganov, *Biophys. Chem.*, 2007, **127**, 9.
- B. Jacrot, *Rep. Prog. Phys.*, 1976, **39**, 911.
- S. Krueger, *Physica B*, 1998, **241–243**, 1131.
- B. Jacrot, C. Chauvin and J. Witz, *Nature*, 1977, **266**, 417.
- C. Chauvin, P. Pfeiffer, J. Witz and B. Jacrot, *Virology*, 1978, **88**, 138.
- M. Cuillel, C. Berthet-Colominas, P. A. Timmins and M. Zulauf, *Eur. Biophys. J.*, 1987, **15**, 169.
- M. Leimkuhler, A. Goldbeck, M. D. Lechner and J. Witz, *J. Mol. Biol.*, 2000, **296**, 1295.
- J. Kruse, P. A. Timmins and J. Witz, *Virology*, 1982, **119**, 42.
- R. K. Heenan, J. Penfold and S. M. King, *J. Appl. Crystallogr.*, 1997, **30**, 1140.
- S. M. King, 1999, *Small-angle Neutron Scattering in: Modern Techniques for polymer characterisation* (Chichester, UK: John Wiley & Sons Ltd.).
- J. K. Blasie and P. Timmins, *MRS Bulletin*, 1999, **24**, 40.

-
- 46 K. E. van Holde, W. C. Johnson and P. S. Ho, 1998, *Principles of Physical Biochemistry* (New Jersey Prentice Hall: Upper Saddle River).
- 47 P. Zipper and H. Durchschlag, *J. Appl. Crystallogr.*, 2007, **40**, S153.
- 48 R. K. Heenan, 1989. *Fish Data Analysis Program: Report RAL-89-129* (Rutherford Appleton Laboratory: Didcot, Oxfordshire), and www.small-angle.ac.uk.
- 49 M. Kotlarchyk and S.-H. Chen, *J. Chem. Phys.*, 1983, **79**, 2461.
- 50 J. Krüse, K. M. Krüse, J. Witz, C. Chauvin, B. Jacrot and A. Tardieu, *J. Mol. Biol.*, 1982, **162**, 393.
- 51 J. Tang, J. M. Johnson, K. A. Dryden, M. J. Young, A. Zlotnick and J. E. Johnson, *J. Struct. Biol.*, 2006, **154**, 59.
- 52 K. W. Adolph and P. J. Butler, *J. Mol. Biol.*, 1974, **88**, 327.